

## Large-scale Propagation of Very Light Jets in Galaxy Clusters

V. Gaibler, M. Camenzind

*Landessternwarte, ZAH, Königstuhl 12, 69117 Heidelberg, Germany*

M. Krause

*Astrophysics Group, Cavendish Laboratory, Madingley Road, Cambridge CB3 0HE, United Kingdom*

**Abstract.** We performed MHD simulations of very light bipolar jets with density contrasts down to  $10^{-4}$  in axisymmetry, which were injected into a medium of constant density and evolved up to 200 kpc ( $200 r_j$ ) full length. These jets show weak and roundish bow shocks as well as broad cocoons and thermalize their kinetic energy very efficiently. We argue that very light jets are necessary to match low-frequency radio observations of radio lobes as well as the bow shocks seen in X-rays. Due to the slow propagation, the backflows and their turbulent interaction in the midplane are important for a realistic global appearance.

### 1. Introduction

During the last years, simulations of extragalactic jets with reasonable resolution and realistic sizes became computationally feasible, which makes comparisons between simulated and observed properties possible (Saxton et al. 2002; Zanni et al. 2003; Carvalho et al. 2005; Krause 2005; O’Neill et al. 2005). Unfortunately, the direct physical variables and the observed properties are rather hard to link, which leaves simulations with a wide range of parameters. Simulations are mainly governed by the initial setup of the density ratio between jet and ambient gas, the Mach number and the magnetic field. If the magnetic field is not dynamically dominant (though important), the density contrast is the most dominant parameter, but may be one of the hardest to measure. The thermal jet pressure has turned out to be of little importance in the very light jet limit (Krause 2003). As the (kinetic) power of a jet can be estimated from energies in X-ray bubbles, typical values of velocity, lifetime, jet radius and cluster gas densities indicate that density contrasts of  $10^{-2}$  to  $10^{-4}$  (or even lower) are necessary to describe real sources. Parameter studies support this further, if the global jet/cocoon/bow shock properties are compared. Thus, we concentrate on the very light jets with magnetic fields as another important ingredient.

### 2. Numerical Method and Setup

We examine the evolution of the jets in axisymmetric simulations using the non-relativistic MHD code NIRVANA (Ziegler & Yorke 1997) and evolve the mag-

netic fields using the constrained transport method, which conserves  $\nabla \cdot \mathbf{B}$  to machine roundoff errors.

Simulations of very light hydro and MHD jets were performed with density contrasts  $\eta = \rho_j/\rho_a$  between  $10^{-4}$  and  $10^{-1}$  where the jet density is  $\rho_j$  and the ambient gas has a constant density of  $\rho_a$ . We will focus on the MHD jets, as their hydro counterparts are only for comparison. The bipolar jet was injected along the Z axis in cylindrical coordinates with a jet radius of  $r_j = 1$  kpc, the jet speed and the sound speed were fixed at  $0.6 c$  and  $0.1 c$  respectively (which gives internal Mach number 6). The ambient gas has a density of  $0.01 m_p/\text{cm}^3$  and a temperature of  $5 \times 10^7$  K. Fully ionized hydrogen was assumed for both the jet and the external medium. The MHD simulations have an initial dipolar field in the whole domain with  $\sim 20 \mu\text{G}$  at the jet boundary and a temporally constant toroidal field with  $\sim 15 \mu\text{G}$  which is confined to the nozzle. For the  $10^{-3}$  and especially the  $10^{-4}$  jet, the magnetic fields thus become dynamically important and influence the appearance. The simulations were run until they reach the boundary of the grid which has  $(4000 \times 800)$  or  $(4000 \times 1600)$  cells (depending on the density contrast) and the jet radius is resolved with 20 cells.

### 3. Morphology

Density and temperature distribution for a  $\eta = 10^{-3}$  jet is shown in Fig. 1. The jet backflow blows up a pronounced cocoon, surrounded by a thick shell of shocked ambient matter. Ambient gas is mixed into the cocoon in finger-like structures due to Kelvin-Helmholtz instabilities at the contact surface. Near the jet heads, this instability is suppressed by the magnetic field, which leads to a smoother appearance there. In purely hydrodynamic simulations, this stabilization is absent. As observations at low radio frequencies show quite smooth contact discontinuities, this indicates the importance of magnetic fields there.

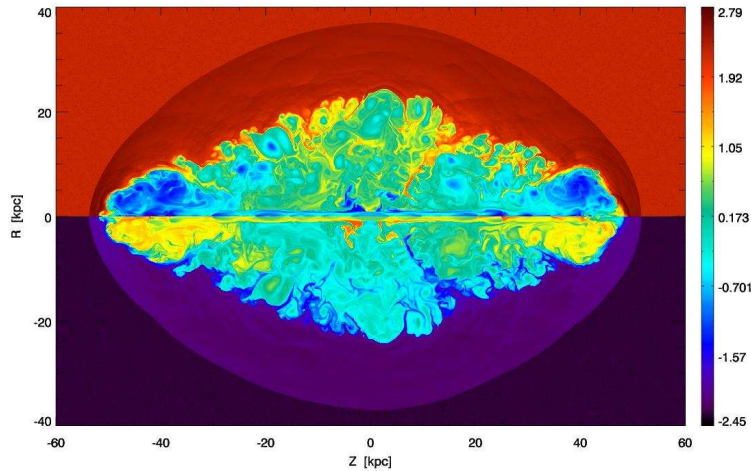


Figure 1. Density and temperature for a bipolar jet with  $\eta = 10^{-3}$  after 15 Myrs. The upper panel shows the density in units of  $10^{-28} \text{ g/cm}^3$ , the lower one shows the logarithm of temperature in units of  $10^{10} \text{ K}$ .

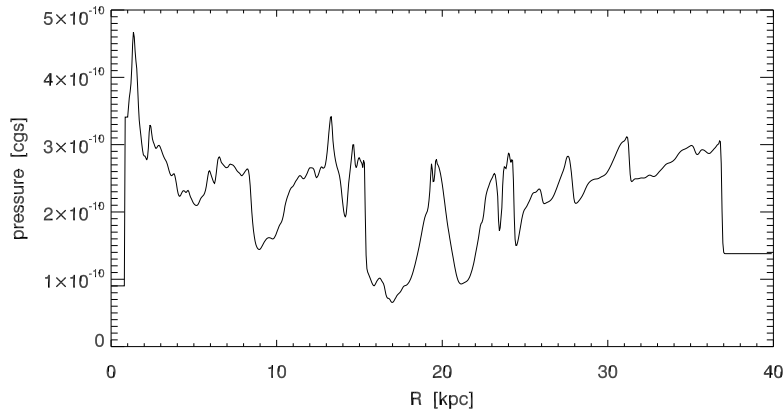


Figure 2. Pressure slice through the  $\eta = 10^{-3}$  jet at  $Z = 0$  after 15 Myr (as Fig. 3). The bow shock is located at  $R \approx 37$  kpc.

The cocoon is highly turbulent and vortices hitting the jet beam can easily destabilize and disrupt it for low jet densities. The Mach numbers quickly decrease and there is no classical “Mach disk” anymore – the terminal shock moves back and forth and isn’t well-defined.

Because very light jets only propagate slowly, the backflow is strong and the turbulence makes the interaction between both jets in the midplane important. These jets have to be simulated bipolarly to get the lateral expansion and hence the global appearance right. If only one jet was simulated, the result would strongly depend on the boundary condition in the equatorial plane (as shown in Saxton et al. 2002).

Outside of the contact surface is the shocked ambient gas, which is pushed outwards by the cocoon pressure. The bow shock for very light jets is different in its shape and strength from that of heavier jets (see section 5.). It is additionally changed by a density profile in the external medium (Krause 2005), which increases the aspect ratio with time and shows cylindrical cocoons.

As example, a radial pressure slice at  $Z = 0$  is shown for the  $10^{-3}$  jet (Fig. 2). The pressure jump at  $R \approx 37$  kpc is the bow shock and is pretty weak compared to bow shocks in heavier jets. Shock speed, pressure and density jump, consistently with the shock jump conditions, give a Mach number of 1.4.

Observations of bow shocks (e.g. Hercules A in Nulsen et al. 2005), which are possible with modern X-ray telescopes, show low Mach numbers and low ellipticity, thus supporting the necessity for very light jet parameters. To find the right cocoon shapes, for comparison low-frequency radio observations have to be chosen, because at higher frequencies only a small part of the cocoon is visible as radio lobes (cooled-down electron population in the backflow is invisible at these frequencies).

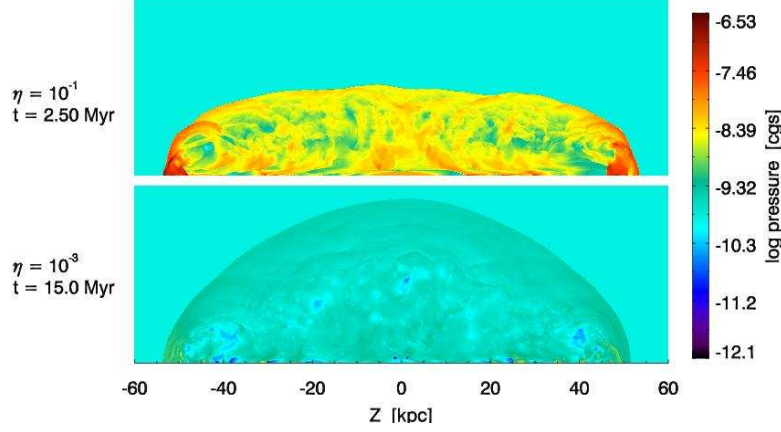


Figure 3. Pressure maps for a  $\eta = 10^{-1}$  and a  $10^{-3}$  jet with the same lengths. The pressure is shown logarithmically in  $\text{dyne}/\text{cm}^2$ . The heavier jet is still much overpressured with respect to the ambient gas and has a much more elongated bow shock compared to the elliptically-shaped bow shock for the lighter jet.

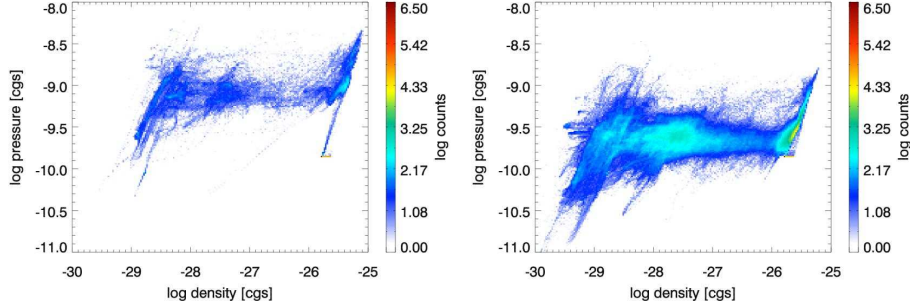


Figure 4. Pressure vs. density histogram for a  $10^{-3}$  jet after 2 Myr (left panel) and 15 Myr (right panel). Cell counts, pressure and density are shown logarithmically using cgs units.

#### 4. Pressure Evolution

The pressure slice shows many variations in Fig. 2, which is not surprising if one looks at the turbulent motion and the mixing inside the cocoon in Fig. 1. Strong pressure waves travel through the cocoon and try to find pressure balance. This process is much more effective for very light jets due to the much slower jet head propagation and it leads to a rather spherical expansion of the bow shock, just like an overpressured bubble. The cocoon of the  $10^{-1}$  jet in Fig. 3 is overpressured by a factor of 20 with respect to the ambient gas, while being a factor of only 1.5 for the  $10^{-3}$  jet (and 4.9 for this jet at  $t = 2.5$  Myr).

This can also be seen in the pressure–density diagrams in Fig. 4. The ambient gas is described by the patch near  $(-26, -10)$ , the jet nozzle by the cells around  $(-29, -10)$ . Adiabatic compression and expansion leads to the oblique and longish features present at different positions. Top right of the jet

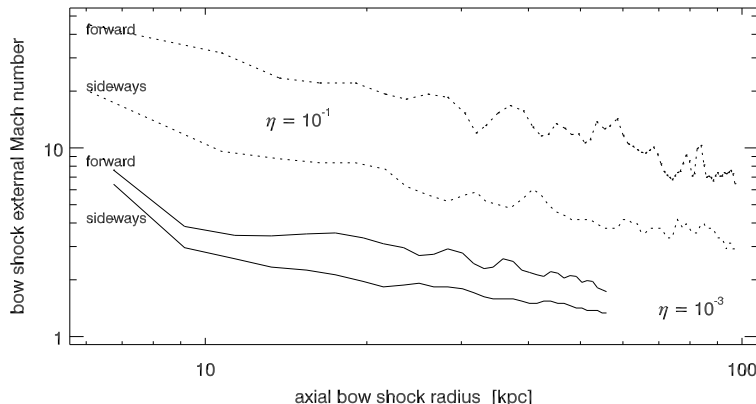


Figure 5. Evolution of the forward and sideways bow shock strength for density contrasts  $\eta = 10^{-1}$  (dotted) and  $10^{-3}$  (solid) as a function of the monotonically increasing axial bow shock radius.

nozzle position are the cocoon grid points, which spread over a large range of density to the right because of mixing with shocked ambient gas, which is the elongated feature top right of the ambient gas position. Comparing the two different simulation snapshots, we find that the pressure distribution is quickly adjusting towards the external pressure, in agreement to the findings in Krause (2003).

## 5. Bow Shock and Cocoon

The quick decrease in cocoon pressure naturally affects the strength of the bow shock as it is this pressure that drives the shock sideways. Fig. 5 shows the temporal evolution of the bow shock strength, in terms of external Mach numbers, for the forward ( $R = 0$ ) direction as well as the sideways ( $Z = 0$ ) direction for jets with different density contrasts. For easier comparison with observations, the axial bow shock radius is used for the abscissa instead of time (but both increase monotonically).

The bow shocks in forward direction are always stronger than the sideways shocks due to the direct impact of the jet onto the ambient gas. The lighter jet has a much weaker bow shock in all directions and the differences between the two directions shown are much less pronounced. The axial diameter of the bow shock increases proportionally to  $t^{0.68}$  after a slower growth during the first 2 Myr, the width grows similarly as  $t^{0.64}$ . An exponent of 0.6 is expected for the blast wave expansion with constant jet power (Krause 2003), while the slower growth rate in the initial phase behaves more like a Sedov blast wave (fixed initial energy amount, exponent is 0.4).

The cocoons, measured by their full (bipolar) lengths and their full Z-averaged widths, grow like the bow shock in axial direction ( $\propto t^{0.71}$ ), but much slower in width ( $\propto t^{0.38}$ ). This leads to a continuously increasing bow shock vs. cocoon width ratio (Fig. 6) with a very thick layer of shocked ambient gas. This effect is weak for heavier jets, but more pronounced the lighter the jet is.

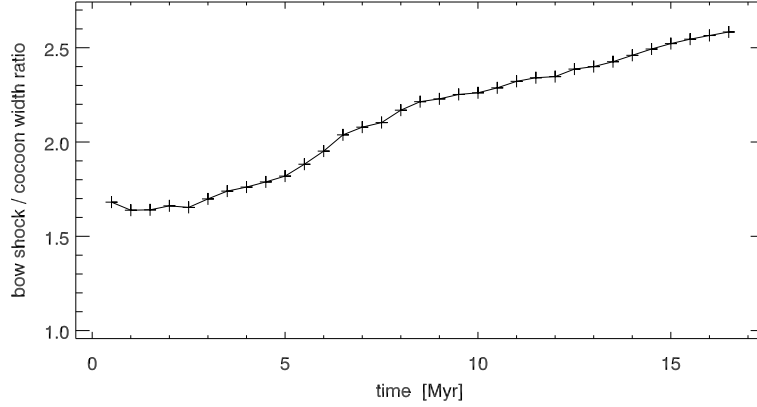


Figure 6. Bow shock / cocoon width ratio over time for a  $10^{-3}$  jet.

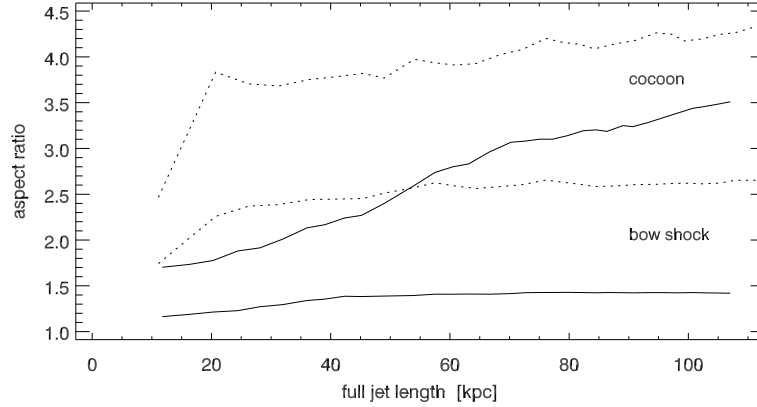


Figure 7. Aspect ratios over full jet length. Dotted line:  $10^{-1}$  jet, solid:  $10^{-3}$  jet. In each case, the lower lines refer to the bow shock and the upper ones to the cocoon.

The aspect ratios (length/width) for the  $10^{-1}$  and  $10^{-3}$  jets are plotted in Fig. 7. The bow shock for the lighter jet starts with a roughly spherical shape and only slightly increases its aspect ratio (length/width) to a constant value of 1.4 (Fig. 7). The heavier jet behaves similarly but approaches a much higher aspect ratio of 2.6. Thus the aspect ratio of the bow shock may be a good property to compare with observations. The aspect ratio of the cocoons in contrast continues to increase, with the heavier jet being on much higher values at all times.

## 6. Thermalization

From the quick adjustment of pressure towards an average value, one might expect a strong conversion of the (kinetic) jet power to thermal energy. This, in fact, is measured for our simulations. Already for the heavy  $10^{-1}$  jet, on

average 67 % of the total energy input is measured as thermal energy increase and only 33 % as kinetic energy increase. For the  $10^{-2}$  jet this is 72 % vs. 27 %, and for the  $10^{-3}$  jet already 81 % of the jet power appear as thermal energy increase with 16 % going into kinetic energy. Here, already 2 % go into an increase in magnetic energy, because with lower density the magnetic fields of constant values become more and more important. The  $10^{-4}$  simulation showed a thermalization efficiency of 94 %, but the fractions for kinetic and magnetic energy are now governed by the strong magnetic pressure and will be examined in the future.

The overall trend to very efficient thermalization for low-density jets nicely suits the increasingly spherical bow shock shape due to (isotropic) cocoon pressure. It also provides the cluster with a huge amount of thermal energy and high-entropy plasma, which may be relevant for the problem of cluster heating and cooling flows (eg. Magliocchetti & Brüggen 2007).

**Acknowledgments.** This work was also supported by the Deutsche Forschungsgemeinschaft (Sonderforschungsbereich 439).

## References

- Carvalho, J. C., Daly, R. A., Mory, M. P., & O’Dea, C. P. 2005, *ApJ*, 620, 126  
 Krause, M. 2003, *A&A*, 398, 113  
 Krause, M. 2005, *A&A*, 431, 45  
 Magliocchetti, M., & Brüggen, M. 2007, *MNRAS*, 528  
 Nulsen, P. E. J., Hambrick, D. C., McNamara, B. R., Rafferty, D., Birzan, L., Wise, M. W., & David, L. P. 2005, *ApJ*, 625, L9  
 O’Neill, S. M., Tregillis, I. L., Jones, T. W., & Ryu, D. 2005, *ApJ*, 633, 717  
 Saxton, C. J., Sutherland, R. S., Bicknell, G. V., Blanchet, G. F., & Wagner, S. J. 2002, *A&A*, 393, 765  
 Zanni, C., Bodo, G., Rossi, P., Massaglia, S., Durbala, A., & Ferrari, A. 2003, *A&A*, 402, 949  
 Ziegler, U., & Yorke, H. W. 1997, *Computer Physics Communications*, 101, 54